

**The Distance to the Cygnus Loop from *Hubble Space Telescope*
Imaging of the Primary Shock Front¹**

William P. Blair², Ravi Sankrit², John C. Raymond³, Knox S. Long⁴

Received _____; accepted _____

arXiv:astro-ph/9906015v1 1 Jun 1999

¹Based on observations with the NASA/ESA *Hubble Space Telescope*, obtained at the Space Telescope Science Institute, which is operated by the Association of Universities for Research in Astronomy, Inc., under NASA contract NAS5-26555.

²Department of Physics and Astronomy, 3400 N. Charles St., The Johns Hopkins University, Baltimore, MD 21218

³Harvard-Smithsonian Center for Astrophysics, 60 Garden St., Cambridge, MA 02138

⁴Space Telescope Science Institute, 3700 San Martin Drive, Baltimore, MD 21218

ABSTRACT

We present a *Hubble Space Telescope*/WFPC2 narrow-band H α image of a region on the northeastern limb of the Cygnus Loop supernova remnant. This location provides a detailed example of where the primary blast wave first encounters the surrounding interstellar medium. The filament structure is seen in exquisite detail in this image, which was obtained primarily as an EARLY ACQUISITION image for a follow-up spectroscopic program. We compare the *HST* image to a digitized version of the POSS-I red plate to measure the proper motion of this filament. By combining this value for the proper motion with previous measurements of the shock velocity at this position we find that the distance to the Cygnus Loop is 440 (+130, -100) pc, considerably smaller than the canonical value of 770 pc. We briefly discuss the ramifications of this new distance estimate for our understanding of this prototypical supernova remnant.

Subject headings: ISM: individual (Cygnus Loop) — ISM: nebulae — ISM: supernova remnants — Shock waves

1. Introduction

The Cygnus Loop supernova remnant (SNR) is an extremely important laboratory for studying many astrophysical phenomena related to shock waves and their interaction with the interstellar medium (ISM). Its proximity, its large angular size, and relatively small foreground extinction all help make it an important object for studies across the entire electromagnetic spectrum. Our thoughts and understanding about the Cygnus Loop and what it represents have evolved dramatically over the last several decades, culminating in the current picture, recently summarized by Levenson et al. 1997, of a cavity explosion of a fairly massive star.

Yet while our understanding of the Cygnus Loop has evolved dramatically, there are other aspects of this important object that remain more in the realm of folklore and seem to carry on from one generation to the next. One of these aspects is the distance to the Cygnus Loop, which is an important and basic datum that affects nearly every other aspect or interpretation of this object. The oft-quoted value of this parameter is 770 pc, attributed to Minkowski 1958. He performed a velocity ellipse analysis of 37 filaments and used the proper motion measured by Hubble 1937 of $0''.03 \text{ yr}^{-1}$ for the bright optical filaments to determine this value. Except for occasional “heretical” suggestions such as those of Sakibov & Smirnov 1983 (1.4 kpc) and Braun & Strom 1986 (460 pc), nearly all other researchers have assumed Minkowski’s value for the distance.

In this paper, we derive a new distance to the Cygnus Loop based on *HST* observations of a single filament on the extreme northeastern limb of the remnant. We obtain a proper motion for the filament by comparing the *HST* data to a digitized version of the POSS-I red plate, and use previous data on this filament’s shock velocity to constrain the distance. We briefly discuss the ramifications of this new distance estimate for previous studies of this important object.

2. Observations and Data Reduction

The filament we have observed in the Cygnus Loop has been studied a number of times previously with other instruments and ground-based telescopes (e.g. Raymond et al. 1983; henceforth RBF, Fesen & Itoh 1985, Long et al. 1992 and Hester, Raymond & Blair 1994; henceforth HRB). Located at RA = $20^h56^m28.7$ and Dec = $31^\circ56'39''.1$ (J2000), it is on the extreme northeastern edge of the Cygnus Loop, about $5'$ ahead of the bright radiative filaments seen in this region. This is a region of so-called ‘nonradiative’ shock front where the primary blast wave is encountering partially neutral preshock material (cf. RBF). The X-ray emission from the Cygnus Loop is bounded by these faint Balmer-dominated shock fronts, as can be seen in the data presented by HRB and Levenson et al. 1997.

The imaging data reported in this paper were obtained on 1997 Nov. 16 with the WFPC2 camera on the *Hubble Space Telescope*. The image was obtained primarily for use as an EARLY ACQ exposure, as part of our Cycle 7 *HST* STIS campaign on this same filament. However, we expected the image to be interesting scientifically as well, and devoted three orbits out of our program for this purpose. We have worked directly with the calibrated data extracted from the Guest Observer tape provided by the STScI, using tasks available in the IRAF/STSDAS environment⁵. The SNR filament was placed so that it crossed the WF2 and WF3 CCDs. We used two exposures per orbit and the F656N filter, which is centered near the Balmer H α line. The positioning was offset by $\Delta x = \Delta y = 10$ WFC pixels ($1''$) between each orbit. The two exposures from each orbit were combined individually to remove most of the cosmic ray events. Then the first and third orbit data

⁵IRAF is distributed by the National Optical Astronomy Observatories, which is operated by the Association of Universities for Research in Astronomy, Inc. (AURA) under cooperative agreement with the National Science Foundation. The Space Telescope Science Data Analysis System (STSDAS) is distributed by the Space Telescope Science Institute.

were shifted to align with the data from the second orbit, and the three orbits of data combined into the final image. This produced an image clear of cosmic rays and camera hot pixels, although some effects from the ‘gutter’ between the WF2 and WF3 chips are still visible when the resulting data are displayed at high contrast. The total integration time was 7400 s. Since stellar contamination is not severe and the filament is known to emit primarily in $H\alpha$, no other filters were used.

Figure 1 shows a 720 by 1484 pixel ($72''0$ by $148''4$) region from the combined data. In this image, north is toward the upper right corner (position angle 30.24° from vertical) and east to the upper left, as indicated. The brightest star at lower left is *HST* GSID 0269203438 at $V=13.3$ and position $RA = 20^h56^m7^s.41$ and $Dec = 31^\circ55' 35''.70$ (J2000). The filament stretches across the image as a ribbon of light, with variable intensity along both its length and width. Here we see the primary Cygnus Loop shock wave as a nearly edge-on sheet, gently rolling along our line of sight as it encounters very slightly differing preshock densities. We see no hard kinks or twists in the shock front that would be indicative of larger density contrast features (or a cloud/intercloud type morphology *ala* McKee & Ostriker 1977). Rather, it appears that the brightness variations over the observed region are dominated by line of sight effects, with brighter regions corresponding to deeper columns and/or multiple shock crossings along a given line of sight. The crispest regions of edge-on shock material are at or below our ability to resolve with the $0''.1$ pixels of the WFPC2 Wide Field CCDs. Since the $H\alpha$ emission is expected to be formed very close behind the shock front ($< 10^{14}$ cm; cf. RBF03), we are truly seeing a ‘snapshot’ of the Cygnus Loop shock front as it encounters the preshock medium. Several exceedingly faint filaments are seen in projection behind the primary shock (toward the bottom in Figure 1). These filaments presumably arise from other locations on the primary shock front seen in projection. Their extreme faintness may be due to lower preshock densities or lower neutral fractions in the preshock gas at those positions, or it may simply be that the path length

through the emitting region is smaller.

3. Analysis

In contrast to Minkowski 1958, we determine the distance to the Cygnus Loop based on the properties of just a single filament. To do this we use the best value for the shock velocity at the observed position and a measurement of the proper motion of the filament. For measuring the proper motion we compare our *HST* image with a digitized version of the POSS-I red plate taken about 44 years earlier. We discuss these topics in the sections below.

3.1. Constraints on the Shock Velocity

The Balmer line emission from nonradiative shocks, such as the one we are considering, comes from neutral atoms that pass through the shock front and are collisionally excited by electrons before becoming ionized (Chevalier & Raymond 1978; Chevalier, Kirshner & Raymond). In this zone immediately behind the shock front, a significant fraction of the neutral hydrogen atoms undergo charge exchange with the hot post-shock ions. This results in the Balmer lines having two distinct components - a narrow component with a thermal width representative of the pre-shock temperature and a broad component with a velocity spread representative of the post-shock ion temperature. Since the post-shock ion temperature depends on the shock velocity, the width of the broad component of the $H\alpha$ line is a diagnostic for the shock velocity.

The translation of the width of the broad component of the $H\alpha$ line to an actual shock velocity depends upon the equilibration mechanism between ions and electrons in the post-shock region. The shock energy thermalizes 3/4 the bulk velocity of the pre-shock

particles so the increase in the temperature of the ions is higher than the increase in the temperature of the electrons by the ratio of their masses. The temperatures eventually come into equilibrium via Coulomb collisions. However, if there is rapid equilibration between the ions and electrons, for instance via plasma turbulence within the shock front (or some other mechanism), then the increase in ionic temperature is lower than otherwise. Therefore, a given width of the broad $H\alpha$ line implies a higher shock velocity for the case of rapid equilibration.

The two component line structure has been observed for the filament we are discussing, but with somewhat discrepant results. RBF used the Whipple 1.5 m telescope and echelle spectrograph and a $2''.5$ by $7''.5$ aperture oriented east-west across the central portion of the filament. They determined $\Delta v_{narrow} = 31 \text{ km s}^{-1}$ and $\Delta v_{broad} = 167 \text{ km s}^{-1}$, which implies that the shock velocity is 170 km s^{-1} for the case of Coulomb equilibration and 210 km s^{-1} for rapid equilibration. Later HRB used the Kitt Peak 4 m telescope with a long slit ($200''$ by $1''.2$) echelle oriented nearly along the length of the filament (see HRB Figure 4). The width of the narrow component in their spectrum agrees with the RBF value. However, they found $\Delta v_{broad} = 130 \pm 15 \text{ km s}^{-1}$, significantly lower than the RBF value. The inferred shock velocity is then 130 km s^{-1} for Coulomb equilibration and 165 km s^{-1} for rapid equilibration.

Geometric considerations can also affect the observed broad component width. Slight non-tangencies (especially both into and out of the plane of the sky combined) would be expected to widen the measured broad component width compared with truly edge-on. Any such broadening in the observed profiles for this filament must indeed be very symmetrical, owing to the well-centered narrow $H\alpha$ component in both the RBF and HRB data sets. HRB estimated the extent of non-tangencies to be $\sim 6^\circ$ (plus and minus to keep the broad and narrow components centered), a number that is consistent with the apparent bumps

and wiggles viewed *along* the filament in Figure 1. The widening occurs as the sine of this angle, allowing of order 20% broadening from geometric effects (worst case). Reconstructing the RBF and HRB slits onto the resolved image in Figure 1 shows a high filling factor of very nearly edge-on shock material in the HRB slit and a larger fraction of non-tangent shock material in the RBF slit. This is in the right direction to account for much of the observed difference in broad component width, and perhaps indicates the RBF shock velocity estimates (e.g. 170 – 205 km s⁻¹) are on the high side.

A different set of diagnostics for the shock velocity is the strength of lines from high ionization species arising further downstream from the H α zone. Since the ionization is due to collisions, the highest ionization stage reached by any element depends on the temperature of the post-shock gas which in turn depends on the shock velocity. Also these lines are formed further downstream where Coulomb collisions have in any case had time to equilibrate the ion and electron temperatures, so their strengths are not as sensitive to the equilibration mechanism. The filament under discussion here was observed with the *Hopkins Ultraviolet Telescope* (Long et al. 1992) and its spectrum showed strong O VI $\lambda\lambda$ 1032,1038 and N V $\lambda\lambda$ 1239,1243 emission. By comparing the observed line strengths with shock model calculations, Long et al. 1992 found that the spectrum could be best fit by shock models with velocities 175 to 185 km s⁻¹. Lower shock velocities could not produce the observed O VI emission and higher shock velocities resulted in an unacceptably high ratio of O VI to N V emission.

As HRB and Long et al. 1992 discuss, their observations can be reconciled if either the shock front is rapidly decelerating, or if there is rapid equilibration of ions and electrons in a 170 km s⁻¹ shock front. If the shock is indeed decelerating, then the shock velocity appropriate for the last 50 years needs to be used in calculating the distance to the remnant. If the deceleration is so rapid that the velocity changes significantly over a period of 50

years, that also would need to be accounted for.

Given the uncertainties discussed above, we adopt $v_{shock} = 170 \pm 20 \text{ km s}^{-1}$ as a reasonable estimate for the relevant shock velocity, and use this in the distance calculation below.

3.2. A New Proper Motion Measurement

We determine the proper motion of the filament by comparing our *HST* image with a digitized scan of the POSS-I red plate of the region. This scan, kindly provided by the Catalogs and Surveys Branch at STScI, was performed with $15 \mu\text{m}$ pixels, corresponding to $1''.0$ per pixel. The POSS image was taken on 1953 July 14 and the *HST* image on 1997 November 16, giving us a temporal separation of 16195 days ($1.40 \times 10^9 \text{ s}$) between the two epochs.

We obtain the proper motion of the filament by measuring the perpendicular distance between selected stars and the local shock front in both POSS and *HST* images. At the resolution of the POSS image, the shock looks smooth. In contrast, the *HST* image shows that the shock front has very complicated substructure. Therefore for our comparison we have convolved the *HST* image with a Gaussian of $\text{FWHM} = 5''.4$, which corresponds to the point spread function determined for stars in the POSS image. In Figure 2 we show two locations where intensity profiles were taken along cuts passing through the shock front and a suitable star. In each case, the leftmost panel shows the POSS image, the middle panel shows the smoothed *HST* image and the right panel shows the original *HST* image. (The regions shown in the POSS images have the same size as the regions in the *HST* images - all are $74'' \times 72''$ although the alignments differ by about 20°). The intensity profiles were taken along the length of the boxes shown, and averaged over the width.

The results of our measurements are shown in Figure 3. For each location, we have plotted the background subtracted, normalized intensity profile along the cuts shown in Figure 2. The dotted line shows the POSS profile and the dashed line the profile from the smoothed *HST* image. The star positions have been aligned, and the advance of the shock front is clearly visible. For Position 1 (top panel), the shock front has advanced by $3''.5$ and for Position 2 (bottom panel) by $3''.6$.

Our use of stars as fiducials in measuring the proper motion of the shock front is justified only if the stars themselves do not have a high proper motion. The best way to test for this effect would be to obtain astrometric solutions based on independently determined positions of stars in the field. Unfortunately, there is only one catalogued star in the field of view of the HST image. Therefore, we have used the information in the respective FITS file headers to obtain astrometric solutions for both the digitized POSS and HST images and compared the displacement of our fiducial stars relative to a set of 14 other stars in the field. We find that the nominal changes in coordinates for our fiducial stars are not abnormal compared with other field stars. The standard deviation in the relative proper motion for all the stars is $\sim 0''.5$. For the specific stars used in our analysis, we find that the positional changes are $0''.5$ and $0''.2$ for the stars used at Position 1 and 2, respectively. The magnitude of errors thus introduced in the measurement of shock proper motion is similar to those due to other factors, as we discuss below.

Despite the poor resolution of the POSS image, this method should give reasonably accurate results if the substructure of the shock has not changed drastically between the two observations, and it is reassuring that the results for two different locations give very similar values for the proper motion. To examine the effects of changes in the filament substructure, we took a profile from the full resolution HST image and changed the intensities of substructures within the shock front in arbitrary ways and saw how that

affected the location of the peak in the smoothed profile. We found that fairly extreme changes in the substructure, such as completely eliminating the second strongest peak in the Position 1 profile (ahead of the brightest band, see Figure 2), changed the derived proper motion by about $0''.5$. Another possible source of error is that we have taken profiles which are perpendicular to an “average” shock front. To estimate errors caused by profiles not being normal to the local shock front, we compared profiles at slightly different angles (passing through the same star) and found that the derived proper motion could vary by about $0''.3$. Experiments with several other methods and crosscuts at numerous other positions (using stars much farther from the local shock front) all gave answers consistent with those given above, typically within a few tenths of an arcsecond. Hence, we adopt a value for the filament proper motion of $3''.6 \pm 0''.5$ in 16195 days (~ 44 years) for use below.

3.3. Revised Distance to the Cygnus Loop

The above velocity and proper motion can now be converted into a distance, under the assumption that the motion of the filament is directly transverse to the line-of-sight. This assumption cannot be far off for several reasons, including the appearance of the filament, its position on the extreme limb of the SNR, and the fact that the narrow Balmer line components in spectral data are well-centered on the broad components (cf. HRB). For our best estimate values of $v_{shock} = 170 \text{ km s}^{-1}$ and proper motion = $3''.6$, we find $d = 442 \text{ pc}$. Applying the uncertainties on these parameters as discussed above, we derive an allowed range of $342 - 573 \text{ pc}$ (where the higher number corresponds to the high velocity – small proper motion limit and vice versa). We note that either a) substantial deceleration of this shock front over the time period of the measurement, b) widening of the observed broad Balmer component due to shock front geometry, or c) some combination of both would only *lower* the appropriate velocity and hence *decrease* this distance estimate. These

uncertainties can clearly be reduced further, both by obtaining a second epoch of *HST* imaging data at some point and by better understanding of the electron – ion equilibration and possible deceleration of the shock front.

It should be noted that the shock velocity estimates implicitly assume that the kinetic energy dissipated in the shock front is transformed into thermal energy of the ions and electrons. If a large fraction of the shock energy is used to accelerate cosmic rays, a higher shock speed is required. Boulares & Cox 1988 present a cosmic ray dominated shock model for the filament in question with a shock speed of 365 km s^{-1} . However, the shock precursor in this model reaches far too high a temperature to be consistent with the $\text{H}\alpha$ profile (HRB), and it is likely that only $\sim 10\%$ of the shock energy goes into non-thermal particles. Thus consideration of cosmic ray acceleration might increase the v_{shock} estimate by 5% .

While considerable uncertainty remains in the distance estimate, it is clear that the canonical value of 770 pc is no longer tenable. It is of interest to note that Braun & Strom 1986 concluded $d = 460 \pm 160 \text{ pc}$ more than a decade ago, based on Hubble’s (1937) and Minkowski’s (1958) original data but fitting for the best *mean* expansion velocity instead of using the extreme of the velocity ellipse (as done by Minkowski). Also, Shull & Hippelein 1991 estimated a distance of 600 pc, but with a large uncertainty that extended upward and downward by a factor of two. Taken in this light, the distance derived here is not out of line with the existing measurements for the bright filaments.

4. Concluding Remarks

A distance of $\sim 440 \text{ pc}$ to the Cygnus Loop has some obvious and important ramifications for the determination of the Cygnus Loop’s basic physical properties. Quantities that depend linearly on distance should be reduced by a factor of ~ 0.6 , while

properties depending on d^2 will decrease by a factor of three. At a distance of 440 pc, $1'' = 0.6 \times 10^{16}$ cm and the angular dimensions of the Cygnus Loop (2.8° by 3.5° ; cf. Levenson et al. 1997) corresponds to linear dimensions of 21.5 pc by 27 pc. Hence, the fact that the crispest regions of edge-on shock in Figure 1 reduce to a single WFC pixel or less places an upper limit of 0.6×10^{15} cm on the size of the $H\alpha$ emitting region behind the shock, still in keeping with expectations (cf. RCFG). Centered at galactic latitude -8.6° , a z distance of about 66 ($d/440$) pc is now appropriate, placing the SNR much closer to the galactic mid-plane. The inferred X-ray luminosity (Ku et al. 1984) drops to $L_x(0.1 - 4\text{keV}) = 3.6 \times 10^{34} (d(\text{pc})/440)$ ergs s^{-1} . Other parameters can be similarly adjusted from the literature.

The smaller distance will also have ramifications for models such as the “cavity explosion” picture put forward most recently by Levenson et al. 1997. Since the cavity does not have to be as large, the inferred precursor star does not have to be as early as B0. Also, a smaller radius indicates a smaller age for the SNR would be appropriate. Ku et al. 1984 determine a Sedov age of 18,000 yrs, which reduces to 5000 ($d(\text{pc})/440$) years. Our point here is not to argue for a Sedov model, but to simply point out that, as the “prototypical middle-aged SNR,” perhaps the Cygnus Loop should be considered to be on the young side of middle-aged.

It is interesting to note that another galactic SNR has recently undergone a similar contraction in its distance estimate. The Vela SNR has been assumed to be at a distance of 500 pc for many years, based on a crude estimate by Milne 1968. (Interestingly, this distance estimate was at least partially based on the assumed ‘known’ distance to the Cygnus Loop!) Several author’s over the last decade have provided reason to suspect a closer distance may be appropriate for Vela, and a recent absorption line study to stars of known distance toward Vela (Cha, Sembach, & Danks 1999) solidifies this result: Vela

appears to be at a distance of only 250 pc or so.

That the distances to two of the most intensely studied galactic SNRs could be off by a factor of order two only serves to accentuate the need to exercise caution when performing a comparative analysis of galactic SNRs. At their revised distances, the linear sizes of the Cygnus Loop and Vela are quite similar, and yet their observed optical and X-ray morphologies are quite different from one another. Global evolutionary studies for galactic SNRs will continue to be fraught with uncertainty until distances to individual objects can be determined with reasonable accuracy.

Obviously, a second epoch of *HST* imaging data on this filament in a few years would provide a superior proper motion analysis and allow this result to be refined. Our nominal filament motion estimate of $3''.6$ corresponds to an expected $0''.082$ per year, or more than three WFC pixels motion in four years. Such a comparison would also allow a direct assessment of any changes in relative brightness of the shock front as a function of position and remove any effect of this on the proper motion determination.

We wish to thank Brian McClean, Barry Lasker, and others in the Catalogs and Surveys Branch at STScI for providing the digitized POSS-I data. We also thank the anonymous referee for a timely report with useful suggestions. This work has been supported by STScI grant GO-07289.01-96A to the Johns Hopkins University.

REFERENCES

- Boulares, A., & Cox, D. P. 1988, *ApJ*, 333, 198
- Braun, R., & Strom, R. G. 1986, *A&A*, 164, 208
- Cha, A. N., Sembach, K. S., & Danks, A. C. 1999, *ApJ*, submitted
- Chevalier, R. A. & Raymond, J. C. 1978, *ApJ*, 225, L27
- Chevalier, R. A., Kirshner, R. P. & Raymond, J. C. 1980, *ApJ*, 235, 186
- Fesen, R. A., & Itoh, H. 1985, *ApJ*, 293, 43
- Hester, J. J., Raymond, J. C., & Blair, W. P. 1994, *ApJ*, 420, 721 (HRB)
- Hubble, E. P. 1937, *Carnegie Inst. Yearbook*, No. 36, p. 189
- Ku, W. H-M., Kahn, S. M., Pisarski, R. & Long, K. S. 1984, *ApJ*, 278, 615
- Levenson, N. A., et al. 1997, *ApJ*, 484, 304
- Long, K. S., Blair, W. P., Vancura, O., Bowers, C. W., Davidsen, A. F., & Raymond, J. C.
1992, *ApJ*, 400, 214
- McKee, C. F., & Ostriker, J. P. 1977, *ApJ*, 218, 148
- Milne, D. K. 1968, *Aust. J. Phys.*, 21, 201
- Minkowski, R. 1958, *Rev. Mod. Phys.*, 30, 1048
- Raymond, J. C., Blair, W. P., Fesen, R. A. , & Gull, T. R. 1983, *ApJ*, 275, 636 (RBF)G
- Raymond, J. C., Hester, J. J., Cox, D. P., Blair, W. P., Fesen, R. A. , & Gull, T. R. 1988,
ApJ, 325, 869

Sakibov, S. K., & Smirnov, M. A. 1983, *Sov. AJ*, 27, 395

Shull, P. J. , & Hippelein, H. 1991, *ApJ*, 383, 714

Fig. 1.— *HST*/WFPC2 $H\alpha$ image of a nonradiative filament on the northeast limb of the Cygnus Loop. (Compare to Figure 1 of Long et al. 1992 for a ground-based view.) The region shown is 1484 by 720 pixels ($148''.4$ by $72''.0$); north is at upper right, east to upper left. The shock wave is moving upward in this figure, with the interior of the SNR toward the bottom.

Fig. 2.— Cuts along which intensity profiles have been taken. Top set of images is for Position 1 and bottom set of images is for Position 2. In each case left image is digitized POSS, middle is smoothed *HST* and right is full resolution *HST* showing sub-structure. Note that for position 2, the reference star is very faint in the smoothed *HST* image, but is clearly seen in the full resolution *HST* image.

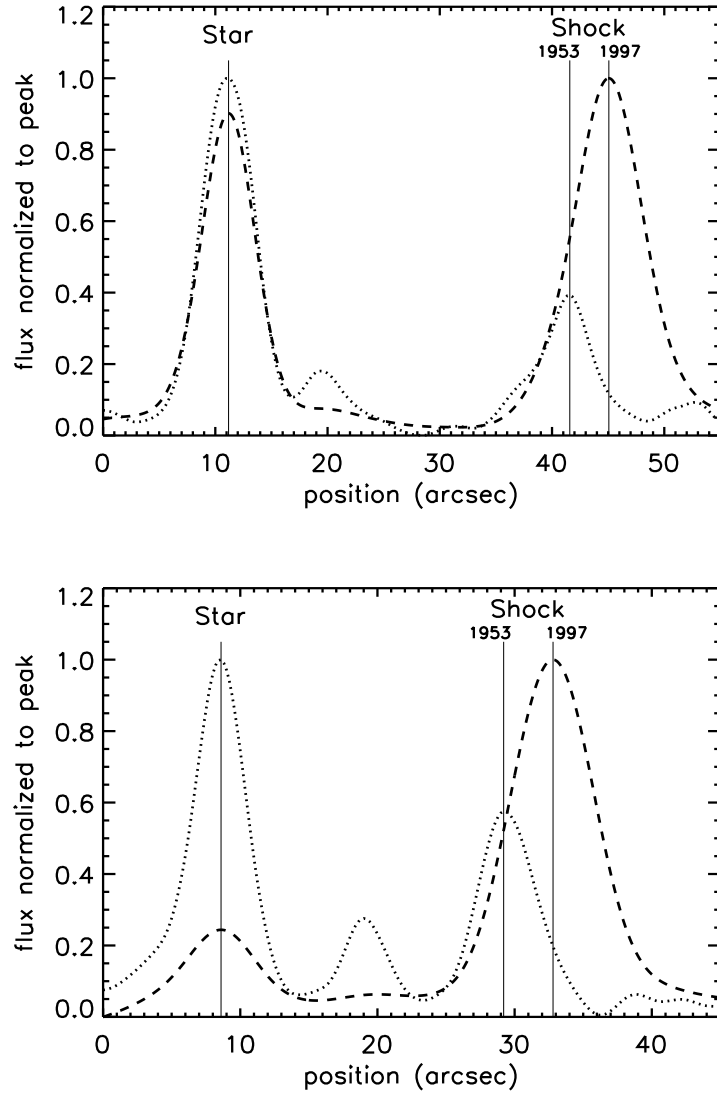


Fig. 3.— Results of proper motion measurements. The top plot is for Position 1 and bottom plot is for Position 2. The measured proper motions are $3''.5$ and $3''.6$, respectively.

This figure "fig1.jpg" is available in "jpg" format from:

<http://arxiv.org/ps/astro-ph/9906015v1>

This figure "fig2.jpg" is available in "jpg" format from:

<http://arxiv.org/ps/astro-ph/9906015v1>